Aerospace Science and Technology 146 (2024) 108975

Contents lists available at ScienceDirect

Aerospace Science and Technology

journal homepage: www.elsevier.com/locate/aescte

GPS-free roll and pitch estimation through pressure altitude aided inertial navigation system for a jet aircraft

Matthew B. Rhudy [a,*], Mario L. Fravolini [b], Marcello R. Napolitano [c]

[a] Division of Engineering, Business, and Computing, The Pennsylvania State University, P.O. Box 7009, Reading, PA 19610-6009, USA
[b] Department of Engineering, University of Perugia, Via G. Duranti N8 93 06125 Perugia, Italy
[c] Department of Mechanical and Aerospace Engineering, West Virginia University, PO Box, 6106, Morgantown, WV 26506, USA

ARTICLE INFO

Keywords:
Altitude estimation
Attitude estimation
Unscented Kalman Filter

ABSTRACT

This paper presents a novel approach for estimating roll and pitch angles of an aircraft by regulating the dead-reckoning drift using pressure altitude measurements. The proposed algorithm uses measurements from rate gyroscopes, pressure altitude, and an air data system to estimate the roll and pitch angles of an aircraft. This unique combination of sensor data offers a new alternative to traditional navigation approaches relying on accelerometers and satellite systems to estimate the aircraft attitude. Multiple flight data sets from a high-speed crewed US Navy T-38 jet are used to validate the proposed approach. Comparable levels of attitude estimation accuracy are reported thus demonstrating that the proposed algorithm is a viable alternative for attitude estimation purposes. Therefore, this approach can be used to improve the robustness and accuracy of attitude estimation algorithms in scenarios where GPS coverage is denied, unreliable, spoofed and/or jammed.

Introduction

Attitude estimation is a key issue for aircraft navigation purposes. Aircraft attitude information is equally important for pilots as well as flight control laws for safe guidance and navigation. Since this information is so safety critical, attitude estimation is an ongoing research topic. There are numerous specific applications requiring accurate knowledge of the aircraft attitude. Autopilot flight control [1], remote sensing [2], and target tracking [3] are just a few applications. Although it is possible to measure aircraft attitude directly, e.g., with a vertical gyroscope, these sensors tend to be large, heavy, and expensive, making them impractical and inefficient in certain scenarios [4]. Due to these restrictions, low-cost attitude estimation has been a popular topic for many years.

A popular basis of many low-cost attitude estimation algorithms is the use of micro-electromechanical systems (MEMS) rate gyroscope measurements. Effectively, the rate gyroscope measurements can be integrated to predict the attitude of the aircraft. However, due to bias errors which commonly occur in MEMS rate gyroscopes [5], the integration typically leads to a drift in the estimated attitude. To address this issue, other sensor systems are used in conjunction with sensor fusion algorithms such as complementary filter or Kalman-based filters to regulate the drift. These types of strategies have been successfully applied to both fixed-wing and multirotor aircraft. This work focuses on the application of low-cost attitude estimation for fixed-wing aircraft, although there are numerous relevant efforts in multirotor attitude estimation, e.g., see [6]. Other aircraft, such as flapping wing aircraft, have also been studied in other works [7].

One of the early strategies commonly implemented for low-cost attitude estimation is Global Positioning System/Inertial Navigation System (GPS/INS) sensor fusion [8]. The basic principle behind this approach is to regulate the attitude estimation drift from rate gyroscope integration by utilizing the relationship between aircraft body frame and the GPS navigation frame through the attitude angles [9]. Various estimation strategies have been implemented for the GPS/INS attitude estimation problem, such as complementary filter [10], Extended Kalman Filter (EKF) [11], Unscented Kalman Filter (UKF) [12], and other more complex variations of these filters, e.g. [13] or [14]. An adaptive Kalman filter with unknown noise statistics was explored in [15].

Due to the possibility of outages in the GPS signal, various researchers have considered alternatives to GPS for regulating the rate gyroscope drift. One common GPS-free attitude estimation strategy is based on the use of vision sensors. One possible way to utilize vision information for attitude estimation is through horizon detection [16]. It has also been shown that wide-field optical flow information from a downward facing camera can be used to extract attitude information without the use of GPS [17]. Some researchers have also combined GPS,

* Corresponding author.
E-mail address: mbr5002@psu.edu (M.B. Rhudy).

https://doi.org/10.1016/j.ast.2024.108975
Received 27 June 2023; Received in revised form 4 December 2023; Accepted 8 February 2024
Available online 12 February 2024

Nomenclature

b_p	Roll rate bias state [rad/s]
b_q	Pitch rate bias state [rad/s]
b_r	Yaw rate bias state [rad/s]
C_b^n	Rotation matrix from the navigation frame to the aircraft body frame
EKF	Extended Kalman Filter
$\mathbf{f}$	Discrete time state transition function
$\mathbf{f}_c$	Continuous time state transition function
g	Acceleration due to gravity [m/s^2]
GPS	Global Positioning System
$\mathbf{H}$	Observation matrix
$\mathbf{h}$	Observation function
h	Altitude [m]
INS	Inertial Navigation System
$\mathbf{I}$	Identity matrix
$\mathbf{K}$	Kalman gain matrix
L	Dimension of augmented state vector for UKF
$L_{\mathbf{f}}$	Lie derivative with respect to $\mathbf{f}_c$
NED	North-East-Down coordinate frame
n_x	Dimension of the state vector
n_y	Dimension of the output vector
n_u	Dimension of the input vector
$\mathbf{O}$	Observability matrix
$\mathbf{P}$	State error covariance matrix
p	Roll rate [rad/s]
$\mathbf{Q}$	Process noise covariance matrix
q	Pitch rate [rad/s]
$\mathbf{R}$	Measurement noise covariance matrix
r	Yaw rate [rad/s]
T_s	Sampling time [s]
t	Continuous time [s]
UKF	Unscented Kalman Filter
$\mathbf{u}$	Input vector
u	Velocity component in the aircraft body x-direction [m/s]
V	Airspeed [m/s]
$\mathbf{v}$	Measurement noise vector
v	Velocity component in the aircraft body y-direction [m/s]
$\mathbf{w}$	Process noise vector
w	Velocity component in the aircraft body z-direction [m/s]
w_p	Process noise term corresponding to roll rate
w_q	Process noise term corresponding to pitch rate
w_r	Process noise term corresponding to yaw rate
w_V	Process noise term corresponding to airspeed
w_α	Process noise term corresponding to angle of attack
w_β	Process noise term corresponding to sideslip angle
w_{b_p}	Process noise term corresponding to roll rate bias
w_{b_q}	Process noise term corresponding to pitch rate bias
w_{b_r}	Process noise term corresponding to yaw rate bias
$\mathbf{x}$	State vector
$\mathbf{y}$	Output vector
$\mathbf{z}$	Measurement vector
z	Down position coordinate in a North-East-Down frame [m]
α	Angle of attack [rad]
α_{UKF}	Primary scaling parameter for Unscented Kalman Filter
β	Sideslip angle [rad]
β_{UKF}	Secondary scaling parameter for Unscented Kalman Filter
θ	Pitch angle [rad]
κ_{UKF}	Tertiary scaling parameter for Unscented Kalman Filter
σ^2	Variance
ϕ	Roll angle [rad]
χ	Sigma-point for Unscented Kalman Filter

IMU, and vision information to further improve the attitude estimation performance [18].

Other attitude estimation strategies rely on only Inertial Measurement Unit (IMU) signals, which often include accelerometers, magnetometers, and rate gyroscopes. Researchers have considered the use of the complementary filter using only IMU measurements to estimate the attitude [19]. A GPS-free attitude estimation algorithm was developed using only accelerometers and magnetometers in [20]. There are some other research publications describing attitude estimation algorithms without using the rate gyroscopes, such as [21] and [22]. Other strategies consider the use of aircraft dynamic model information to aid in the estimation of attitude [22]. Alternative sensor systems have also been considered for regulating rate gyroscope drift using infrared sensors [23].

One piece of information that is commonly measured on many aircraft but not often considered within attitude estimation algorithms is the altitude. It is common for altitude to be calculated through pressure measurements; however, this information has limited application to attitude estimation algorithms. A barometer measurement was implemented as part of a larger estimation algorithm in [24], but this technique included many other sensor packages as well. Another work considered barometric pressure measurements for correcting position information during GPS outages [25].

This work proposes a novel attitude estimation algorithm which utilizes pressure altitude measurements as the primary means of regulating the attitude drift experienced from rate gyroscope integration. The contributions of this work can be summarized as follows:

1. A novel algorithm for GPS-free attitude estimation is proposed; the scheme relies only on rate gyroscope, pressure altitude, and air data measurements.
2. The algorithm is implemented using an UKF and EKF with non-additive noise modelling to accurately characterize the measurement errors in the model equations.
3. The proposed method is independent of the aircraft dynamic model: therefore, without any loss of generality, it can be applied to different types of fixed wing aircraft, including both crewed and uncrewed aircraft.
4. The proposed method is validated with respect to multiple sets of experimental flight data from a crewed US Navy T-38 jet.

The paper is organized as follows. Section 2 presents the proposed estimation algorithm and description of the considered experimental setup. Section 3 details the flight data results and discussion of these results in context. A brief conclusion is offered in Section 4.

Materials and methods

Structure for the attitude and altitude estimation filter

A state estimation filter considers the use of state space equations with a state vector, $\mathbf{x}$, input vector, $\mathbf{u}$, and output vector, $\mathbf{y}$, such that the continuous time nonlinear state space equations are given by:

$$\begin{aligned}\dot{\mathbf{x}}(t) &= \mathbf{f}_c(\mathbf{x}(t), \mathbf{u}(t), \mathbf{w}(t)) \\ \mathbf{y}(t) &= \mathbf{h}(\mathbf{x}(t), \mathbf{u}(t), \mathbf{v}(t))\end{aligned} \tag{1}$$

where $\mathbf{f}_c$ is the continuous time vector-valued state prediction function,

h is the observation function, **w** is the non-additive process noise vector, and **v** is the non-additive measurement noise vector. Here, the non-additive noise model is used since it is a more general case than the commonly assumed additive noise assumption. The purpose of a state estimator is to estimate the state vector, **x**, using information provided by the input vector, **u**, and measurements of the output vector, **y**. Thus, the "output" of the filter is estimates of the state vector, **x**. The state space model of the attitude estimation filter is formulated as follows:

$$\begin{aligned}\mathbf{x} &= [\,\phi \quad \theta \quad h \quad b_p \quad b_q \quad b_r\,]^T,\\ \mathbf{u} &= [\,p \quad q \quad r \quad V \quad \alpha \quad \beta\,]^T,\\ \mathbf{y} &= [h].\end{aligned} \tag{2}$$

where ϕ is the roll angle, θ is the pitch angle, h is the altitude; p, q, r are the roll, pitch, and yaw rates, respectively, with corresponding bias states b_p, b_q, b_r. Here, bias states are considered for the rate gyroscope signals because estimating these biases aids in the reduction of the drift the occurs when integrating the rate gyroscope signals due to bias errors. The airspeed is denoted by V, while the angle of attack and sideslip angle are denoted by α and β, respectively. The output is a direct measurement of the altitude state through the pressure altitude measurement, thus resulting in a simple linear measurement update. The rate gyroscope and air data information are formulated as inputs in this model since this information is necessary to predict the state dynamics of the system. Since the pressure measurement is a measurement signal that is not prone to drift, it provides the necessary reference to regulate the integrated state space equations. The dimensions of the state, input, and output vectors are denoted by $n_x = 6$, $n_u = 6$, and $n_y = 1$, respectively.

The state dynamics for the roll and pitch angle states are provided through the inverse kinematic equations [26], as in:

$$\begin{aligned}\dot{\phi} &= p + q\sin\phi\tan\theta + r\cos\phi\tan\theta\\ \dot{\theta} &= q\cos\phi - r\sin\phi\end{aligned} \tag{3}$$

The dynamics for the altitude state can be determined by utilizing the rotation matrix from the navigation frame to the aircraft body frame:

$$C_b^n = \begin{bmatrix} \cos\theta\cos\psi & -\cos\phi\sin\psi + \sin\phi\sin\theta\cos\psi & \sin\phi\sin\psi + \cos\phi\sin\theta\cos\psi \\ \cos\theta\sin\psi & \cos\phi\cos\psi + \sin\phi\sin\theta\sin\psi & -\sin\phi\cos\psi + \cos\phi\sin\theta\sin\psi \\ -\sin\theta & \sin\phi\cos\theta & \cos\phi\cos\theta \end{bmatrix} \tag{4}$$

Next, the position dynamics can be described using this rotation matrix to relate the aircraft velocity in aircraft body components (u, v, w), to North-East-Down (NED) components ($\dot{x}, \dot{y}, \dot{z}$), as in:

$$\begin{bmatrix} \dot{x} \\ \dot{y} \\ \dot{z} \end{bmatrix} = C_b^n \begin{bmatrix} u \\ v \\ w \end{bmatrix} \tag{5}$$

The aircraft body velocity components can also be expressed in terms of the airspeed, angle of attack, and sideslip angle, as in:

$$\begin{bmatrix} u \\ v \\ w \end{bmatrix} = \begin{bmatrix} V\cos\alpha\cos\beta \\ V\sin\beta \\ V\sin\alpha\cos\beta \end{bmatrix} \tag{6}$$

Then, the z-velocity component can be isolated as:

$$\dot{z} = V(-\cos\alpha\cos\beta\sin\theta + \sin\beta\sin\phi\cos\theta + \sin\alpha\cos\beta\cos\phi\cos\theta) \tag{7}$$

The z-position state was considered as "down" in the NED framework. Therefore, in order to obtain the altitude state dynamics, a sign change is necessary, resulting in the following dynamics for altitude:

$$\dot{h} = V(\cos\alpha\cos\beta\sin\theta - \sin\beta\sin\phi\cos\theta - \sin\alpha\cos\beta\cos\phi\cos\theta) \tag{8}$$

Note that this altitude state dynamic equation neglects the effect of vertical wind.

Nonlinear state estimation using nonlinear kalman filtering

Due to the nonlinearity in the state dynamics equations for the roll, pitch, and altitude states, a nonlinear state estimation technique is necessary. Here, both EKF and UKF are considered and compared, since each one offers different advantages and disadvantages [27]. Due to the use of rate gyroscope measurements as well as air data measurements in the input vector, a non-additive noise model was assumed for the system. Thus, the following nonlinear discrete-time state space system was utilized:

$$\begin{aligned}\mathbf{x}_k &= \mathbf{f}(\mathbf{x}_{k-1}, \mathbf{u}_{k-1}, \mathbf{w}_{k-1})\\ \mathbf{y}_k &= \mathbf{h}(\mathbf{x}_k, \mathbf{u}_k, \mathbf{v}_k)\end{aligned} \tag{9}$$

where k is the discrete time index, **f** is the discrete-time vector-valued state prediction function, **h** is the nonlinear vector-valued observation function, **w** is the non-additive process noise vector, and **v** is the non-additive measurement noise vector. For this particular system, the observation equations are a direct measurement of the state, resulting in a simple linear system update with additive measurement noise, as in:

$$\begin{aligned}\mathbf{y}_k &= \mathbf{H}_k\mathbf{x}_k + \mathbf{v}_k\\ \mathbf{H}_k &= [\,0 \quad 0 \quad 1 \quad 0 \quad 0 \quad 0\,]\end{aligned} \tag{10}$$

where the measurement noise vector is due to uncertainty in the pressure altitude measurement, as in:

$$\mathbf{v} = v_h \tag{11}$$

The state dynamics were given in continuous time in (3) and (8); thus, a first order discretization is used to put into a discrete time format, as in:

$$\mathbf{x}_k = \mathbf{x}_{k-1} + T_s\mathbf{f}_c(\mathbf{x}_{k-1}, \mathbf{u}_{k-1}, \mathbf{w}_{k-1}) = \mathbf{f}(\mathbf{x}_{k-1}, \mathbf{u}_{k-1}, \mathbf{w}_{k-1}) \tag{12}$$

where T_s is the sampling time, which for this work is 0.05 s to correspond to a 20 Hz sampling frequency. Incorporating the non-additive noise terms and rate gyroscope bias states leads to the following stochastic discrete-time state prediction equations for roll, pitch, and altitude:

$$\begin{aligned}\phi_k &= \phi_{k-1} + T_s(\widehat{p}_{k-1} + \widehat{q}_{k-1}\sin\phi_{k-1}\tan\theta_{k-1} + \widehat{r}_{k-1}\cos\phi_{k-1}\tan\theta_{k-1})\\ \theta_k &= \theta_{k-1} + T_s(\widehat{q}_{k-1}\cos\phi_{k-1} - \widehat{r}_{k-1}\sin\phi_{k-1})\\ h_k &= h_{k-1} + T_s\widehat{V}_{k-1}\begin{pmatrix}\cos\widehat{\alpha}_{k-1}\cos\widehat{\beta}_{k-1}\sin\theta_{k-1} - \sin\widehat{\beta}_{k-1}\sin\phi_{k-1}\cos\theta_{k-1}\\ -\sin\widehat{\alpha}_{k-1}\cos\widehat{\beta}_{k-1}\cos\phi_{k-1}\cos\theta_{k-1}\end{pmatrix}\end{aligned} \tag{13}$$

where the $\widehat{\ }$ terms indicate the corresponding input terms after removing the bias state and considering non-additive noise, as in:

$$\begin{aligned}\widehat{p} &= p - b_p + w_p, \quad \widehat{V} = V + w_V\\ \widehat{q} &= q - b_q + w_q, \quad \widehat{\alpha} = \alpha + w_\alpha\\ \widehat{r} &= r - b_r + w_r, \quad \widehat{\beta} = \beta + w_\beta\end{aligned} \tag{14}$$

The rate gyroscope bias states are predicted using random walk, which is a commonly implemented model for IMU bias states, as in:

$$\begin{aligned}b_{p,k} &= b_{p,k-1} + w_{b_p}\\ b_{q,k} &= b_{q,k-1} + w_{b_q}\\ b_{r,k} &= b_{r,k-1} + w_{b_r}\end{aligned} \tag{15}$$

The resulting process noise vector is provided by:

$$\mathbf{w} = \begin{bmatrix} w_p & w_q & w_r & w_V & w_\alpha & w_\beta & w_{b_p} & w_{b_q} & w_{b_r} \end{bmatrix}^T \tag{16}$$

Then, the process and measurement noise covariance matrices can be represented by:

$$\begin{aligned}\mathbf{Q} &= diag\begin{bmatrix}\sigma_{w_p}^2 & \sigma_{w_q}^2 & \sigma_{w_r}^2 & \sigma_{w_V}^2 & \sigma_{w_\alpha}^2 & \sigma_{w_\beta}^2 & \sigma_{w_{b_p}}^2 & \sigma_{w_{b_q}}^2 & \sigma_{w_{b_r}}^2\end{bmatrix}\\ \mathbf{R} &= \sigma_{v_h}^2\end{aligned} \tag{17}$$

where each of the individual variance terms are considered to be zero-mean uncorrelated Gaussian noise. The measurement noise covariance matrix, $\mathbf{R}$, here consists of a single term that corresponds to the uncertainty in the pressure altitude measurement.

Using these definitions, the UKF for non-additive noise can be implemented. Due to the linear observation equations, the linear KF update can be used in this case. The UKF equations are presented with more details in [28] and are summarized here for this particular application.

For non-additive process noise, the state vector of the UKF can be augmented with additional "states" to model the non-additive process noise terms, as in

$$\mathbf{x}_k^a = \begin{bmatrix} \mathbf{x}_k \\ \mathbf{w}_k \end{bmatrix} \tag{18}$$

where the superscript 'a' denotes the augmentation. The error covariance matrix must also be augmented accordingly, taking the form of a block diagonal matrix

$$\mathbf{P}_k^a = \begin{bmatrix} \mathbf{P}_k & \mathbf{0} \\ \mathbf{0} & \mathbf{Q}_k \end{bmatrix} \tag{19}$$

Now, the augmented state vector and covariance matrix are used to generate the augmented sigma-points

$$\begin{aligned} \boldsymbol{\chi}_{k-1}^a &= \begin{bmatrix} \boldsymbol{\chi}_{k-1}^x \\ \boldsymbol{\chi}_{k-1}^w \end{bmatrix} \\ &= \begin{bmatrix} \widehat{\mathbf{x}}_{k-1}^a & \widehat{\mathbf{x}}_{k-1}^a + \sqrt{L+\lambda_{UKF}}\sqrt{\mathbf{P}_{k-1}^a} & \widehat{\mathbf{x}}_{k-1}^a - \sqrt{L+\lambda_{UKF}}\sqrt{\mathbf{P}_{k-1}^a} \end{bmatrix} \end{aligned} \tag{20}$$

where L is the dimension of the augmented state vector, and λ_{UKF} is an UKF scaling parameter, defined as

$$\begin{aligned} &\lambda_{UKF} = \alpha_{UKF}^2(L+\kappa_{UKF}) - L \\ &\boldsymbol{\eta}_0^m = \lambda_{UKF}/(L+\lambda_{UKF}) \\ &\boldsymbol{\eta}_0^c = \lambda_{UKF}/(L+\lambda_{UKF}) + 1 - \alpha_{UKF}^2 + \beta_{UKF} \\ &\boldsymbol{\eta}_i^m = \boldsymbol{\eta}_i^c = 1/[2(L+\lambda_{UKF})], \quad i = 1, ..., .2L \end{aligned} \tag{21}$$

where α_{UKF}, β_{UKF}, and κ_{UKF} are the primary, secondary, and tertiary UKF scaling parameters. The $\boldsymbol{\eta}$ terms are weight vectors used to recover the mean and covariance after the nonlinear transformation. The sigma-points can be separated into two sections, that is state, $\mathbf{x}$, and process noise, $\mathbf{w}$, as noted by the superscripts. Now, only the state sigma-points need to be predicted using prior information from both the state and process noise sigma-points

$$\boldsymbol{\chi}_{k|k-1}^{x,(i)} = f\left(\boldsymbol{\chi}_{k-1}^{x,(i)}, \mathbf{u}_{k-1}, \boldsymbol{\chi}_{k-1}^{w,(i)}\right), i = 0, 1...., 2L \tag{22}$$

The *a priori* statistics are then recovered using

$$\begin{aligned} \widehat{\mathbf{x}}_{k|k-1} &= \sum_{i=0}^{2L} \boldsymbol{\eta}_i^m \boldsymbol{\chi}_{k|k-1}^{x,(i)} \\ \mathbf{P}_{k|k-1} &= \sum_{i=0}^{2L} \boldsymbol{\eta}_i^c \left(\boldsymbol{\chi}_{k|k-1}^{x,(i)} - \widehat{\mathbf{x}}_{k|k-1}\right)\left(\boldsymbol{\chi}_{k|k-1}^{x,(i)} - \widehat{\mathbf{x}}_{k|k-1}\right)^T \end{aligned} \tag{23}$$

Since the measurement equations are linear, the linear Kalman filter update can be used

$$\begin{aligned} &\mathbf{K}_k = \mathbf{P}_{k|k-1}\mathbf{H}_k^T\left(\mathbf{K}_k\mathbf{P}_{k|k-1}\mathbf{H}_k^T + \mathbf{R}_k\right)^{-1} \\ &\widehat{\mathbf{x}}_k = \widehat{\mathbf{x}}_{k|k-1} + \mathbf{K}_k\left(\mathbf{y}_k\mathbf{H}_k\widehat{\mathbf{x}}_{k|k-1}\right) \\ &\mathbf{P}_k = (\mathbf{I} - \mathbf{K}_k\mathbf{H}_k)\mathbf{P}_{k|k-1} \end{aligned} \tag{24}$$

where $\mathbf{K}$ is the Kalman gain matrix and $\mathbf{I}$ is an identity matrix of appropriate dimensions.

The EKF can also use the linear measurement update but uses different methodology for determining the *a priori* statistics:

$$\begin{aligned} \widehat{\mathbf{x}}_{k|k-1} &= \mathbf{f}(\widehat{\mathbf{x}}_{k-1}, \mathbf{u}_{k-1}, 0) \\ \mathbf{P}_{k|k-1} &= \mathbf{F}_{k-1}\mathbf{P}_{k-1}\mathbf{F}_{k-1}^T + \mathbf{L}_{k-1}\mathbf{Q}_{k-1}\mathbf{L}_{k-1}^T \end{aligned} \tag{25}$$

where the Jacobian matrices are given by:

$$\mathbf{F}_{k-1} = \left.\frac{\partial \mathbf{f}}{\partial \mathbf{x}}\right|_{\widehat{\mathbf{x}}_{k-1}, \mathbf{u}_{k-1}}, \quad \mathbf{L}_{k-1} = \left.\frac{\partial \mathbf{f}}{\partial \mathbf{w}}\right|_{\widehat{\mathbf{x}}_{k-1}, \mathbf{u}_{k-1}} \tag{26}$$

Nonlinear state estimator observability

To investigate the capability of the nonlinear estimators in predicting the roll and pitch angles using the altitude measurement, a nonlinear observability analysis was conducted. The following method was used to conduct the observability analysis, as outlined in [29].

For nonlinear state space systems as defined in (1), the observability can be calculated using Lie derivatives, as in:

$$L_{\mathbf{f}_c}\mathbf{h} = \sum_{i=1}^{n_x} \frac{\partial \mathbf{h}}{\partial \mathbf{x}_i}\mathbf{f}_{c,i} \tag{27}$$

where the zero order Lie derivative is given by

$$L_{\mathbf{f}_c}^0\mathbf{h} = \mathbf{h} \tag{28}$$

and the higher order Lie derivatives are given by

$$L_{\mathbf{f}_c}^j\mathbf{h} = \frac{\partial\left(L_{\mathbf{f}_c}^{j-1}\mathbf{h}\right)}{\partial \mathbf{x}}\cdot\mathbf{f}_{c,i} \tag{29}$$

Then, the observability can be determined by verifying that the observability matrix is full rank

$$\mathbf{O}(\mathbf{x}_k) = \frac{\partial l(\mathbf{x})}{\partial \mathbf{x}} \tag{30}$$

where

$$l(\mathbf{x}_k) = \begin{bmatrix} L_{\mathbf{f}_c}^0\mathbf{h}(\mathbf{x}_k) \\ ... \\ L_{\mathbf{f}_c}^{n_x-1}\mathbf{h}(\mathbf{x}_k) \end{bmatrix} \tag{31}$$

Note that for the considered estimation problem, there is only a single observation in $\mathbf{h}(\mathbf{x}_k)$ which is the altitude, h.

Using this method, and considering the first three states of the filter, ϕ, θ, and h, the Lie derivatives are given by:

$$\begin{aligned} &l_1 = L_{\mathbf{f}_c}^0\mathbf{h} = \mathbf{h} = h \\ &l_2 = L_{\mathbf{f}_c}^1\mathbf{h} = \frac{\partial\left(L_{\mathbf{f}_c}^0\mathbf{h}\right)}{\partial \mathbf{x}}\cdot\mathbf{f}_{c,i} = \frac{\partial h}{\partial \mathbf{x}}\cdot\mathbf{f}_{c,i} = V(c\alpha c\beta s\theta - s\beta s\phi c\theta - s\alpha c\beta c\phi c\theta) \\ &l_3 = L_{\mathbf{f}_c}^2\mathbf{h} = \frac{\partial\left(L_{\mathbf{f}_c}^1\mathbf{h}\right)}{\partial \mathbf{x}}\cdot\mathbf{f}_{c,i} = \begin{array}{l} V(-s\beta c\phi c\theta + s\alpha c\beta s\phi c\theta)(p + qs\phi\tan\theta + rc\phi\tan\theta) \\ \quad + V(c\alpha c\beta c\theta + s\beta s\phi s\theta + s\alpha c\beta c\phi s\theta)(qc\phi - rs\phi) \end{array} \end{aligned} \tag{32}$$

where $c\alpha = \cos(\alpha)$ and $s\alpha = \sin(\alpha)$ and similar for the other angles for brevity. Thus the observability matrix takes the following form

$$\mathbf{O}(\mathbf{x}_k) = \begin{bmatrix} 0 & 0 & 1 \\ \dfrac{\partial l_2}{\partial \phi} & \dfrac{\partial l_2}{\partial \theta} & 0 \\ \dfrac{\partial l_3}{\partial \phi} & \dfrac{\partial l_3}{\partial \theta} & 0 \end{bmatrix} \tag{33}$$

Here, due to the structure of the first row and last column, the problem reduces to making sure the rank of the 2×2 matrix is full rank.

$$\mathbf{O}^{2\times 2}(\mathbf{x}_k) = \begin{bmatrix} \frac{\partial l_2}{\partial \phi} & \frac{\partial l_2}{\partial \theta} \\ \frac{\partial l_3}{\partial \phi} & \frac{\partial l_3}{\partial \theta} \end{bmatrix} \tag{34}$$

The details for these individual derivative terms are provided as follows

$$\frac{\partial l_2}{\partial \phi} = V(-s\beta c\phi c\theta + s\alpha c\beta s\phi c\theta)$$

$$\frac{\partial l_2}{\partial \theta} = V(c\alpha c\beta c\theta + s\beta s\phi s\theta + s\alpha c\beta c\phi s\theta)$$

$$\frac{\partial l_3}{\partial \phi} = \begin{bmatrix} V(s\beta s\phi c\theta + s\alpha c\beta c\phi c\theta)(p + qs\phi \tan\theta + rc\phi \tan\theta) \\ +V(-s\beta c\phi c\theta + s\alpha c\beta s\phi c\theta)(qc\phi \tan\theta - rs\phi \tan\theta) \\ +V(s\beta c\phi s\theta - s\alpha c\beta s\phi s\theta)(qc\phi - rs\phi) \\ +V(c\alpha c\beta c\theta + s\beta s\phi s\theta + s\alpha c\beta c\phi s\theta)(-qs\phi - rc\phi) \end{bmatrix} \tag{35}$$

$$\frac{\partial l_3}{\partial \theta} = \begin{bmatrix} V(s\beta c\phi s\theta - s\alpha c\beta s\phi s\theta)(p + qs\phi \tan\theta + rc\phi \tan\theta) \\ +V(-s\beta c\phi c\theta + s\alpha c\beta s\phi c\theta)(qs\phi + rc\phi)\sec^2\theta \\ +V(-c\alpha c\beta s\theta + s\beta s\phi c\theta + s\alpha c\beta c\phi c\theta)(qc\phi - rs\phi) \end{bmatrix}$$

One way to determine if this matrix is full rank is to calculate the determinant. If the result of the determinant is non-zero, then it is full rank, and therefore the system is observable.

When calculated using flight data for each of the flight data sets, the system was determined to be observable throughout each flight. Analytically, there are possible conditions that could result in the system not being observable. One possible case for this is an airspeed $V = 0$. This is not a concern for fixed-wing aircraft, as a zero airspeed is an unlikely scenario to occur within flight. Another possible case lacking observability is if all angular rates are equal to zero, i.e. $p = q = r = 0$. This situation can occur in flight, however it is not a major concern here, since if the angular rates are all equal to zero, the attitude is expected to be constant. There are other possible flight conditions that can occur which lead to loss of observability, such as $\alpha = \beta = \phi = r = 0$, however these are unlikely scenarios to occur, and not likely to last for any significant amount of time, therefore these should not be a concern for the stability of the considered filtering algorithms.

Experimental setup

The Northrop T-38 Talon is a supersonic jet used for flight training by the United States Air Force, NASA, and the United States Navy. Some background on the history of the T-38 is provided in [30]. The T-38 has been the subject of some research studies, such as for modifying the aerodynamics using wind fences [31] or predicting inlet pressure and temperature distortion [32]. For this study, flight data sets from a T-38 C operated by the United States Navy at the US Navy Test Pilot Flight school at the Patuxent River Naval air base are used. An image of a T-38 C is shown in Fig. 1 [33].

Fig. 1. Image of a T-38 C [33].

The available flight data contains IMU data, air data, Euler attitude angles, and pressure altitude all sampled at 20 Hz. A total of 11 flight data sets from the T-38 aircraft were utilized for this study. The details for each of these individual data sets is provided in Table 1. In addition to these 11 flight data sets, one additional flight data set was used only for the purpose of tuning the noise covariance terms and is not included in any results. GPS data, while included in the data sets, was not used in the implementation of the presented algorithm. While permission was obtained for the use of this flight data for research purposes, the specifications of the sensors were not disclosed by the United States Navy and therefore cannot be presented here.

Results and discussion

Determination of noise parameters

In order to determine the noise parameters for the **Q** and **R** matrices for the UKF, an 'ad-hoc' tuning was performed using a different flight data set than Flights #1–11. In other words, the flight data set that was used for tuning was not used to report results for the study. The resulting error characteristics are summarized in Table 2.

Attitude and altitude estimation results

Using the proposed UKF algorithm, roll angle, pitch angle, and altitude were calculated for each of the 11 flights as outlined in Table 1. The roll and pitch estimates are shown for Flight #1 in Fig. 2 (left) and Flight #2 in Fig. 2 (right). Similarly, the altitude estimates are shown for Flight #1 in Fig. 3 (left) and Flight #2 in Fig. 3 (right), and the roll rate, pitch rate, and yaw rate bias states are shown for Flight #1 in Fig. 4 (left) and Flight #2 in Fig. 4 (right). Fig. 2 and Fig. 3 show that the algorithm is able to closely match the reference data from the Attitude Heading and Reference System (AHRS).

To summarize the results for all 11 flight data sets, the root mean square error (RMSE) statistic was calculated for the UKF and EKF estimated roll and pitch angles with respect to the values obtained from the AHRS, and the UKF and EKF estimated altitude with respect to the pressure altitude measurement. These RMSE results are reported in Table 3. To demonstrate the effectiveness of the algorithm in regulating the attitude drift from rate gyroscope integration, the result of attitude estimates from rate gyroscope integration only (dead reckoning) is shown in Fig. 5 for Flight #1. This flight is used as an example, but other flights have similarly poor roll and pitch estimation results. The calculated RMSE values for roll and pitch angles from rate gyroscope integration are 75.87 ° and 94.31 °, respectively. Note that this performance is unacceptably poor, thus motivating the need for regulation.

Table 1
Description of Flight Data Sets.

Flight #	Start Date	Local Start Time	Data Set Duration (min)
1	6/18/2021	7:16:41 PM	59.6
2	6/22/2021	7:14:49 AM	37.7
3	6/22/2021	8:52:28 AM	54.0
4	7/13/2021	11:33:36 AM	44.1
5	7/27/2021	7:43:59 AM	23.0
6	7/27/2021	7:43:59 AM	23.0
7	1/5/2022	4:13:00 PM	25.0
8	1/24/2022	7:37:32 PM	27.9
9	2/24/2022	9:20:12 AM	19.6
10	2/24/2022	11:48:47 AM	21.6
11	2/28/2022	11:56:58 AM	22.0

Table 2
Assumed Noise Characteristics for UKF Implementation.

Symbol	Value	Units
$\sigma^2_{w_p} = \sigma^2_{w_q} = \sigma^2_{w_r}$	10^{-4}	$(\text{rad/s})^2$
$\sigma^2_{w_V}$	10^{-9}	$(\text{m/s})^2$
$\sigma^2_{w_\alpha} = \sigma^2_{w_\beta}$	10^{-6}	$(\text{rad})^2$
$\sigma^2_{w_{b_p}} = \sigma^2_{w_{b_q}} = \sigma^2_{w_{b_r}}$	10^{-13}	$(\text{rad/s})^2$
$\mathbf{R} = \sigma^2_{v_h}$	10^{4}	$(\text{m})^2$

Discussion

The results for RMSE presented in Table 3 demonstrate that the proposed algorithm can provide estimates of the roll angle to within 3 ° of accuracy (though generally better for most flights), and the pitch angle to less than 2 ° of accuracy. Negligible difference was observed between EKF and UKF, as shown in Table 3, therefore either filter can be used for this application. These negligible differences are an indication that the nonlinearity of the system is relatively small, since the primary difference between EKF and UKF is the linearization technique. The level of accuracy for both filters is reasonable, and comparable to other state-of-the-art attitude estimation algorithms. For example, in [9], Gross et al. compared multiple variations of GPS/INS algorithms for attitude estimation using UAV data with reported errors ranging from ~1–4° in mean absolute error and standard deviation of error for roll and pitch angles. Similar accuracies were reported for attitude estimation using optical flow and INS in [17]. Due to similar levels of attitude estimation performance as GPS/INS and OF/INS fusion algorithms, the proposed method can be considered a viable alternative for attitude estimation.

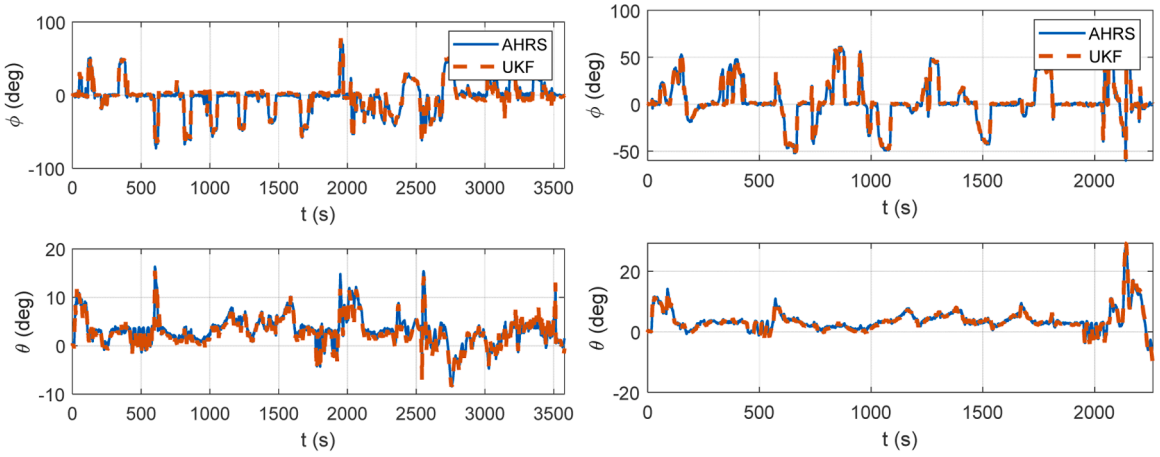

Fig. 2. Estimated Roll and Pitch Angles for Flight #1 (left) and Flight #2 (right).

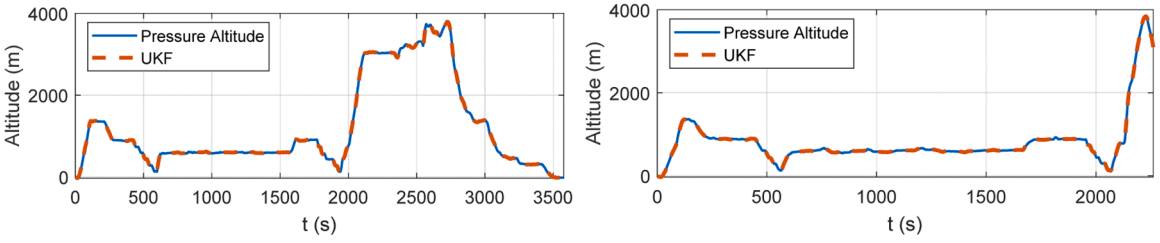

Fig. 3. Estimated Altitude for Flight #1 (left) and Flight #2 (right).

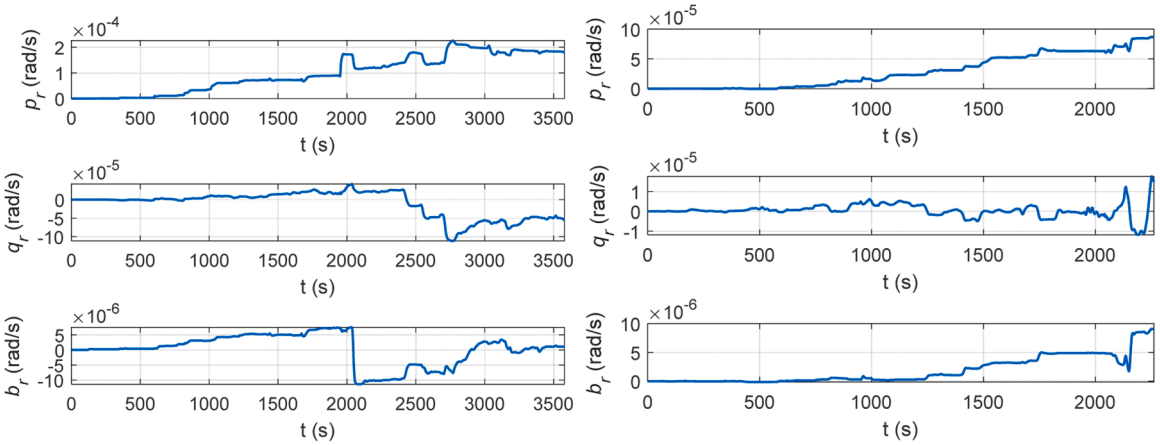

Fig. 4. Estimated Roll Rate, Pitch Rate, and Yaw Rate Bias States for Flight #1 (left) and Flight #2 (right).

Table 3
Roll, Pitch, and Altitude Estimation RMSE Statistics.

Flight #	Roll RMSE (deg)		Pitch RMSE (deg)		Altitude RMSE (m)	
	UKF	EKF	UKF	EKF	UKF	EKF
1	2.952	2.952	0.788	0.788	6.636	6.638
2	0.771	0.770	0.424	0.424	4.660	4.657
3	0.821	0.821	0.470	0.469	3.906	3.905
4	1.331	1.330	1.393	1.393	7.962	7.960
5	1.699	1.699	1.038	1.038	10.653	10.653
6	0.946	0.945	0.639	0.638	10.540	10.532
7	1.341	1.340	0.985	0.984	11.698	11.695
8	2.030	2.029	1.602	1.602	13.617	13.612
9	1.512	1.511	1.261	1.261	13.603	13.601
10	1.522	1.521	1.097	1.097	12.247	12.244
11	1.469	1.468	1.522	1.522	17.501	17.497

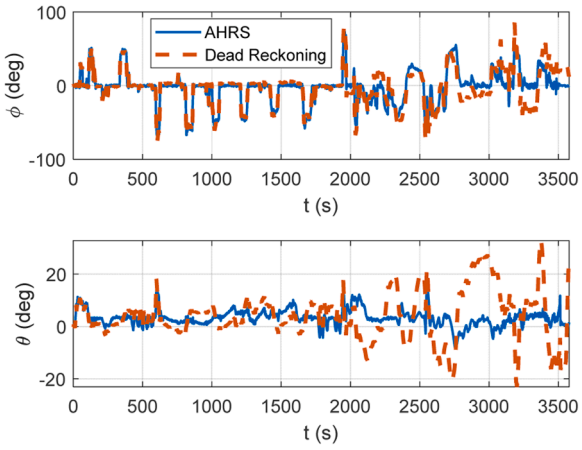

Fig. 5. Dead Reckoning Estimated Roll and Pitch Angles for Flight #1 using only Rate Gyroscope Integration without any Measurement Update from the Pressure Altitude Measurement.

The unique sensor combination offered in this work provides a means for estimating roll and pitch angles without the use of GPS signals or accelerometer sensors. This has multiple potential benefits in different situations. Since the use of pressure altitude for regulating attitude is a novel concept, there is the potential to integrate this idea into new fusion algorithms. This could lead to increasing the robustness of the algorithm to sensor failures or, simply, to improve the overall accuracy of the estimation algorithm. That is, the pressure altitude measurement could be used to regulate attitude in situations where GPS and/or accelerometer sensors are faulty or unreliable. Because most attitude estimation algorithms rely on one or both of these sensors, this type of approach provides a reasonable and valuable alternative to the traditional attitude estimation approaches. Using a navigation approach without accelerometer data allows for the potential to identify and isolate any failures in the accelerometer sensors and/or to handle situations where accelerometer data may not be providing reliable information for attitude estimation purposes. In addition, the pressure altitude measurement is commonly obtained in many aircraft applications, does not require significant payload or computational power to process, and therefore provides a lower-cost and more efficient alternative to vision-based algorithms – which are more computationally intensive - for attitude estimation under GPS failures.

Another potential improvement to this algorithm could be the use of data from a radio altimeter, either as an alternative, or in addition to the pressure altitude measurements. This information could provide additional accuracy and/or robustness to the proposed algorithm and could be considered in future iterations of this type of filtering algorithm.

Conclusions

This work presented a technique for attitude estimation without the use of GPS or accelerometer sensors. The proposed approach is capable of estimating roll and pitch angles to less than 3 ° RMSE accuracy by regulating attitude drift through the use of pressure altitude measurements. This novel approach offers a reasonable alternative to the common GPS/INS approach for attitude estimation for situations where GPS is unavailable or unreliable. In addition, this algorithm could be implemented as an analytical redundancy to help improve the robustness and safety of aircraft sensor systems.

CRediT authorship contribution statement

Matthew B. Rhudy: Conceptualization, Formal analysis, Investigation, Methodology, Software, Validation, Visualization, Writing – original draft, Writing – review & editing. **Mario L. Fravolini:** Conceptualization, Investigation, Methodology, Supervision, Validation, Writing – review & editing. **Marcello R. Napolitano:** Conceptualization, Data curation, Investigation, Project administration, Resources, Supervision, Writing – review & editing.

Declaration of competing interest

The authors declare that they have no known competing financial interests or personal relationships that could have appeared to influence the work reported in this paper.

Data availability

The authors do not have permission to share data.

Funding Statement

The effort described in this article was not funded.

Acknowledgments

The authors would like to thank William P. Geyer, Instructor at the US Navy Test Pilot School at Patuxent River Naval Air Station. Mr. Geyer has provided complete sets of flight data of the US Navy T-38 trainer aircraft.

References

[1] H. Chao, Y. Cao, Y. Chen, Autopilots for small fixed-wing unmanned air vehicles: a survey, in: In 2007 International Conference on Mechatronics and Automation, IEEE, 2007, August, pp. 3144–3149.
[2] L. Changchun, S. Li, W. Hai-bo, L. Tianjie, The research on unmanned aerial vehicle remote sensing and its applications, in: In 2010 2nd International Conference on Advanced Computer Control 2, IEEE, 2010, March, pp. 644–647.
[3] S.L. Liao, R.M. Zhu, N.Q. Wu, T.A. Shaikh, M. Sharaf, A.M. Mostafa, Path planning for moving target tracking by fixed-wing UAV, Defence. Techn. 16 (4) (2020) 811–824.
[4] G. Zhou, D. Zang, Civil UAV system for earth observation, in: In 2007 IEEE International Geoscience and Remote Sensing Symposium, IEEE, 2007, July, pp. 5319–5322.
[5] M. El-Diasty, S. Pagiatakis, A rigorous temperature-dependent stochastic modelling and testing for MEMS-based inertial sensor errors, Sensors 9 (11) (2009) 8473–8489.
[6] S. Liu, P. Lyu, J. Lai, C. Yuan, B. Wang, A fault-tolerant attitude estimation method for quadrotors based on analytical redundancy, Aerosp. Sci. Technol. 93 (2019) 105290.
[7] R. Yang, W. Zhang, J. Mou, B. Zhang, Y. Zhang, Attitude estimation algorithm of flapping-wing micro air vehicle based on extended kalman filter, in: In International Conference on Autonomous Unmanned Systems, Singapore, Springer Nature Singapore, 2022, September, pp. 1432–1443.
[8] M.S. Grewal, L.R. Weill, A.P. Andrews, Global positioning systems, inertial navigation, and integration, John Wiley & Sons, 2007.

[9] J.N. Gross, Y. Gu, M.B. Rhudy, S. Gururajan, M.R. Napolitano, Flight-test evaluation of sensor fusion algorithms for attitude estimation, IEEE Trans. Aerosp. Electron. Syst. 48 (3) (2012) 2128–2139.
[10] M.A. Islam, S. Saha, Loosely coupled GPS/INS integrated navigation system based on Kalman filter and complementary filter for aircraft, in: In 2017 2nd International Conference on Electrical & Electronic Engineering (ICEEE), IEEE, 2017, December, pp. 1–4.
[11] B.P. Duong, V.H. Nguyen, Development of a GPS/INS integrated navigation system for model aircraft, in: In 2014 14th International Conference on Control, Automation and Systems (ICCAS 2014), IEEE, 2014, October, pp. 201–206.
[12] J.L. Crassidis, Sigma-point Kalman filtering for integrated GPS and inertial navigation, IEEE Trans. Aerosp. Electron. Syst. 42 (2) (2006) 750–756.
[13] T. Xiaoqian, Z. Feicheng, T. Zhengbing, W. Hongying, Nonlinear extended kalman filter for attitude estimation of the fixed-wing UAV, Int. J. Opt. (2022) 2022.
[14] G. Hu, W. Wang, Y. Zhong, B. Gao, C. Gu, A new direct filtering approach to INS/GNSS integration, Aerosp. Sci. Technol. 77 (2018) 755–764.
[15] L. Zhang, W.A.N.G. Shaoping, M.S. Selezneva, K.A. Neusypin, A new adaptive Kalman filter for navigation systems of carrier-based aircraft, Chin. J. aeronaut. 35 (1) (2022) 416–425.
[16] A.E.R. Shabayek, C. Demonceaux, O. Morel, D. Fofi, Vision based uav attitude estimation: progress and insights, J. Intell. Robot. Syst. 65 (2012) 295–308.
[17] M.B. Rhudy, Y. Gu, H. Chao, J.N. Gross, Unmanned aerial vehicle navigation using wide-field optical flow and inertial sensors, J. Robot. 2015 (2015).
[18] Z. Zuo, B. Yang, Z. Li, T. Zhang, A GNSS/IMU/vision ultra-tightly integrated navigation system for low altitude aircraft, IEEe Sens. J. 22 (12) (2022) 11857–11864.
[19] R. Mahony, M. Euston, J. Kim, P. Coote, T. Hamel, A non-linear observer for attitude estimation of a fixed-wing unmanned aerial vehicle without GPS measurements, Transact. Inst. Measure. Control 33 (6) (2011) 699–717.
[20] W. Wang, Z. Jin, L. Miao, Z. Yang, S. Mi, Y. Qin, X. Yang, Combined attitude determination for real-time geomagnetic navigation, IEEe Magn. Lett. 13 (2022) 1–5.
[21] A.G. Kallapur, I.R. Petersen, S.G. Anavatti, Robust gyro-free attitude estimation for a small fixed-wing unmanned aerial vehicle, Asian J. Control 14 (6) (2012) 1484–1495.
[22] W. Youn, H. Choi, A. Cho, S. Kim, M.B. Rhudy, Aerodynamic model-aided estimation of attitude, 3-D wind, airspeed, AOA, and SSA for high-altitude long-endurance UAV, IEEE Trans. Aerosp. Electron. Syst. 56 (6) (2020) 4300–4314.
[23] L. Di, T. Fromm, Y. Chen, A data fusion system for attitude estimation of low-cost miniature UAVs, J. Intell. Robot. Syst. 65 (2012) 621–635.
[24] W. Youn, M.B. Rhudy, A. Cho, H. Myung, Fuzzy adaptive attitude estimation for a fixed-wing UAV with a virtual SSA sensor during a GPS outage, IEEe Sens. J. 20 (3) (2020) 1456–1472.
[25] W. Zhao, Z. Fang, P. Li, Bridging GPS outages for fixed-wing unmanned aerial vehicles, J. Navigat. 68 (2) (2015) 308–326.
[26] J. Roskam, Airplane flight dynamics and automatic flight controls, DARcorporation, 1998.
[27] M. Rhudy, Y. Gu, Understanding nonlinear kalman filters part I: selection of EKF Or UKF, Interactive Robotics Letters, 2013.
[28] M. Rhudy, Y. Gu, Understanding nonlinear kalman filters, part II: an implementation guide, Interactive Robotics Letters, 2013.
[29] A. Rouhani, A. Abur, Observability analysis for dynamic state estimation of synchronous machines, IEEE Transact. Power Syst. 32 (4) (2016) 3168–3175.
[30] R. Eden, The northrop grumman t-38 talon-40 years plus and still teaching pilots to fly, in: In 39th Aerospace Sciences Meeting and Exhibit, 2001, p. 313.
[31] M.D. Williams, M.F. Reeder, R.C. Maple, D.A. Solfelt, Modeling, simulation, and flight tests for a T-38 talon with wing fences, J. Aircr. 47 (2) (2010) 423–433.
[32] M.W. Davis Jr, D.S Kidman, Prediction and analysis of inlet pressure and temperature distortion on engine operability from a recent T-38 flight test program, in: In Turbo Expo: Power for Land, Sea, and Air 43963, 2010, October, pp. 1–11.
[33] Alan Wilson from Stilton, Peterborough, Cambs, UK, CC BY-SA 2.0 via Wikimedia Commons, 2016.